Tellus (1984), *36A*, 42–51

The statistical equilibrium solution of a primitive-equation model

By RONALD M. ERRICO, *National Center for Atmospheric Research*[1], *P.O. Box 3000, Boulder, Colorado 80307, U.S.A.*

(Manuscript received February 8; in final form April 25, 1983)

ABSTRACT

The statistical equilibrium solution of an f-plane, primitive-equation model with a single quadratic energy invariant is determined by numerical integration. The initial condition resembles the atmosphere in terms of the shape and magnitude of its energy spectrum. The equilibrium solution is one in which energy is equipartitioned among all the linearly independent modes of the system. This state is attained after two simulated years.

The approach to equilibrium is explored in detail. It is characterized by (at least) two stages. The first is dominated by quasi-geostrophic dynamics and nonlinear balances. The approximate conservation of quasi-geostrophic potential enstrophy is important during this stage, so that the solution initially tends to the equilibrium solution of a quasi-geostrophic form of the model. The second stage is characterized by a very slow transfer of energy from geostrophic modes to inertial-gravity waves. The rate of transfer of energy during this stage is shown to be very sensitive to initial conditions.

1. Introduction

In Errico (1982a) a solution to a very low order, adiabatic, primitive-equation model was presented. Errico's intent was simply to compare the final statistical-equilibrium solution with solutions from diabatic models. Starting from a nearly geostrophic initial condition, he demonstrated that, unlike the diabatic models, the adiabatic one tended to equipartition energy to each independent mode of the system. In particular, ageostrophic motions in the form of gravity waves became as energetic as the geostrophic motions. From this and other experiments, he concluded that dissipation was an important process for the maintenance of approximate geostrophic balance within the atmosphere.

Errico's adiabatic experiment began from an initial condition whose spectra resembled the atmosphere's in shape but not in magnitude. Since details of the approach to equilibrium are expected to depend strongly on the initial strength of the flow (e.g., its energy and enstrophy), he did not discuss the transition to his solution. In particular, he did not try to describe the rate of approach to the final statistically-steady state. This decision was also motivated by consideration of his model's simplicity. For example, due to its sparse-spectral design, it did not include small-scale, nearly-resonant, triad interactions, as would exist either in high resolution models or in the atmosphere. If such interactions allow instabilities, their effects may be initially important in an adiabatic experiment.

In this study, Errico's experiments are repeated using a multi-level spectral model which is not sparse. The initial condition simulates an atmospheric state in amplitude as well as spectral shape. The transient behavior of the solution is examined. In particular, the effect of an initial, nearly geostrophic balance is discussed. While specific resonances are not measured, the importance of non-resonant quasi-geostrophic interactions early in the solution is demonstrated.

[1] The National Center for Atmospheric Research is sponsored by the National Science Foundation.

A model is introduced in Section 2. That is followed by a description of the model's linear normal modes (cf. Leith, 1980). The modes are either geostrophic or ageostrophic, and have specified resonant frequencies. The first experiment with the primitive-equation model is described in Section 4. In Section 5, both a quasi-geostrophic solution and a balance model solution are presented for comparison with the former. Other experiments are described in Section 6. Conclusions, and a comparison with results presented by Frederiksen (1981), are presented in the final section.

2. The model

The primitive-equation (*PE*) model is derived from that of Hoskins and Bretherton (1972). It is both hydrostatic and Boussinesq, and is defined on a periodic f-plane. The vertical coordinate z is a prescribed function of pressure p,

$$z = \left[1 - \left(\frac{p}{p_s}\right)^{\kappa}\right] H_*, \tag{1}$$

where the subscript s denotes a fixed, constant surface value, and $H_* = C_p\theta_0/g$ is the scale height of an isentropic atmosphere with potential temperature θ_0. C_p is the specific heat of air at constant pressure, and $\kappa = R/C_p$, where R is the gas constant.

The model equations are

$$\frac{\partial \mathbf{V}}{\partial t} = -f\mathbf{k} + \mathbf{V} - (\mathbf{V}\cdot\nabla)\mathbf{V} - w\frac{\partial \mathbf{V}}{\partial z} - \nabla\phi, \tag{2}$$

$$\frac{\partial \theta'}{\partial t} = -\mathbf{V}\cdot\nabla\theta' - w\frac{\partial \theta'}{\partial z} - w\alpha, \tag{3}$$

$$\frac{\partial \phi}{\partial z} = g\theta'/\theta_0, \tag{4}$$

$$\frac{\partial w}{\partial z} = -\nabla\cdot\mathbf{V}. \tag{5}$$

The potential temperature has been separated into three components:

$$\theta(x,y,z,t) = \theta_0 + \alpha z + \theta'(x,y,z,t) \tag{6}$$

α is a prescribed (time and space) constant $d\bar{\theta}/dz$. The overbar distinguishes a prescribed z-dependent portion of a field from a prognostic (primed) portion. $\mathbf{V}$ and ∇ are the two-dimensional velocity vector (u,v) and gradient operator, respectively, expressed on surfaces of constant z. t is time. f is the Coriolis parameter. w is the vertical "velocity" dz/dt. ϕ is a perturbation geopotential determined hydrostatically from θ' (that contribution to ϕ by $\theta_0 + \alpha z$ does not affect the dynamics). $\mathbf{k}$ is a vector perpendicular to surfaces of constant z. These equations can also be derived from the primitive equations of Lorenz (1960) if a term $w(1-\kappa)\kappa^{-1}(H_* - z)^{-1}$, which would otherwise appear on the right-hand side of (5), is ignored.

Eqs. (2)–(5) are solved with boundary conditions $w = 0$ at $z = 0$ and $z = \pi H$. This upper boundary condition is somewhat artificial since πH is not specified below as equal to H_*. On any z surface the fields are assumed to be periodic, with fundamental wavelength $2\pi D$. D is set to 1.55×10^6 m. $L = (g\alpha/\theta_0)^{1/2} H/f$ defines a radius of deformation. Here values of $f = 10^{-4}$ s^{-1}, $g = 9.8$ m s^{-2}, $\theta_0 = 290$ K, $\alpha = 0.0045$ K m^{-1}, $C_p = 1000$ m^2 s^{-2} K^{-1}, and $R = 287$ m^2 s^{-2} K^{-1} were used to obtain $H_* = 2.96 \times 10^4$ m, and $L = 3.93 \times 10^5$ m. For comparison with future work, the value $H = (10^4/\pi)$ m was used. The Boussinesq approximation is invalid near $z = H_*$ in any case, so this choice is not too inappropriate.

The numerical version of the model has a pseudo-spectral design by Orszag (personal communication). Solutions are restricted to the form

$$\phi(x,y,z,t) = \sum_{j=-N_j}^{N_j}\sum_{k=-N_k}^{N_k}\sum_{l=0}^{N_l} \hat{\phi}(j,k,l,t) \times \exp[i(jx + ky)/D]\cos(lz/H), \tag{7}$$

$$\hat{\phi}(-j,-k,l,t) = \hat{\phi}^*(j,k,l,t), \tag{8}$$

with similar expressions for $\mathbf{V}$, θ', and w, but with sine replacing cosine for the latter two. The asterisk denotes a complex conjugate. Hereafter, only the spectral coefficients will be referenced, so the caret ($\hat{}$) notation will be dropped. The dependence on the integer indices j, k, l will be denoted by a subscript $\mathbf{K}$.

In the experiments to be described, $N_j = 11$, $N_k = 5$, and $N_l = 5$. All nonlinear terms are calculated on a grid using fast Fourier transforms. The grid has dimensions 32, 16, and 8 in the x, y, and z directions, respectively. This resolution is sufficient to ensure alias-free transforms of quadratic terms.

The integrations in time are performed using

Lorenz's (1971) alternating 4-cycle scheme with a time step of $\Delta t = 250$ s. This scheme is accurate through the d^4/dt^4 term in the Taylor expansion of the variables at time t expressing those at time $t + 4\Delta t$. For Exp. 1, the numerical scheme results in a loss of energy of less than 0.0007% during the first 100 simulated days.

3. Normal modes

The linear normal modes of this model are obtained as the independent solutions of (2)–(5), subject to the spectral forms (e.g. (7)–(8)), and ignoring all quadratic terms (cf. Leith, 1980). Associated with each normal mode is a (linear) resonant frequency. The advantage of using a normal mode description results from this explicit identification and separation of resonant frequencies. The presence or absence of resonant dynamic forcing (due to nonlinearity) greatly affects the solutions.

For each $\mathbf{K} = (j,k,l)$ with $l \neq 0$, there are three modes, whose amplitudes (i.e., coefficients) may be expressed as:

$$g_{\mathbf{K}} = \left(f\zeta_{\mathbf{K}} - \frac{l^2}{L^2}\phi_{\mathbf{K}}\right)\frac{1}{\sqrt{2l\omega_{\mathbf{K}}}}, \tag{9}$$

$$a_{\mathbf{K}} = \left(f\zeta_{\mathbf{K}} + \frac{j^2+k^2}{D^2}\phi_{\mathbf{K}} - i\omega_{\mathbf{K}}\delta_{\mathbf{K}}\right) \times \frac{D}{2\omega_{\mathbf{K}}(j^2+k^2)^{1/2}}, \tag{10}$$

$$d_{\mathbf{K}} = \left(f\zeta_{\mathbf{K}} + \frac{j^2+k^2}{D^2}\phi_{\mathbf{K}} + i\omega_{\mathbf{K}}\delta_{\mathbf{K}}\right) \times \frac{D}{2\omega_{\mathbf{K}}(j^2+k^2)^{1/2}}, \tag{11}$$

where

$$\omega_{\mathbf{K}} = f\left[1 + \frac{L^2}{l^2D^2}(j^2+k^2)\right]^{1/2}, \tag{12}$$

$$\zeta_{\mathbf{K}} = \frac{i}{D}(jv_{\mathbf{K}} - ku_{\mathbf{K}}), \tag{13}$$

$$\delta_{\mathbf{K}} = \frac{i}{D}(ju_{\mathbf{K}} + kv_{\mathbf{K}}). \tag{14}$$

$\zeta_{\mathbf{K}}$ and $\delta_{\mathbf{K}}$ are the vorticity and divergence at scale $\mathbf{K}$, respectively. Since these models have an internal structure, they are called baroclinic. If the fields are geostrophically balanced, then both $a_{\mathbf{K}}$ and $d_{\mathbf{K}}$ are zero for all $\mathbf{K}$. Thus, $g_{\mathbf{K}}$ is called the coefficient for a baroclinic geostrophic mode. $a_{\mathbf{K}}$ and $d_{\mathbf{K}}$ are those for ageostrophic modes.

For each $\mathbf{K} = (j,k,0)$, there is only one mode, whose coefficient may be expressed as

$$b_{\mathbf{K}} = D\zeta_{\mathbf{K}}/[2(j^2+k^2)]^{1/2}. \tag{15}$$

This mode is both geostrophic and barotropic.

The modes associated with $b_{\mathbf{K}}$, $g_{\mathbf{K}}$, $a_{\mathbf{K}}$, and $d_{\mathbf{K}}$ are associated with eigenvalues 0, 0, $-\omega_{\mathbf{K}}$ and $\omega_{\mathbf{K}}$, respectively. Thus, the geostrophic modes are stationary in the linearized model. Only nonlinear effects can change their coefficients. In the linear model, $a_{\mathbf{K}}$ and $d_{\mathbf{K}}$ are amplitudes of inertial gravity waves travelling with phase velocities $\omega_{\mathbf{K}}\, D/(j^2+k^2)^{1/2}$ and $-\omega_{\mathbf{K}}\, D/(j^2+k^2)^{1/2}$, respectively.

The model conserves total energy E (aside from roundoff and time discretization errors) expressed in the form of kinetic energy

$$KE = \frac{1}{2}\sum_{\mathbf{K}}(u_{\mathbf{K}}u_{\mathbf{K}}^* + v_{\mathbf{K}}v_{\mathbf{K}}^*), \tag{16}$$

plus available potential energy

$$PE = \frac{1}{2}\frac{1}{L^2f^2}\sum_{\mathbf{K}} l^2\phi_{\mathbf{K}}\phi_{\mathbf{K}}^*. \tag{17}$$

E can also be expressed in terms of the mode coefficients as

$$E = BE + GE + AE \tag{18}$$

where

$$BE = \tfrac{1}{2}\sum_{\mathbf{K},l\neq 0} b_{\mathbf{K}}b_{\mathbf{K}}^*, \tag{19}$$

$$GE = \tfrac{1}{2}\sum_{\mathbf{K},l\neq 0} g_{\mathbf{K}}g_{\mathbf{K}}^*, \tag{20}$$

$$AE = \tfrac{1}{2}\sum_{\mathbf{K},l\neq 0}(a_{\mathbf{K}}a_{\mathbf{K}}^* + d_{\mathbf{K}}d_{\mathbf{K}}^*). \tag{21}$$

If $a_{\mathbf{K}}$ and $d_{\mathbf{K}}$ are set to zero at each time step, then the model is quasi-geostrophic (QG). In that case, an additional quantity

$$Q = \tfrac{1}{2}\sum_{\mathbf{K},l\neq 0}\frac{j^2+k^2}{D^2}b_{\mathbf{K}}b_{\mathbf{K}}^* + \tfrac{1}{2}\sum_{\mathbf{K},l\neq 0}\left(\frac{l^2}{L_R^2} + \frac{j^2+k^2}{D^2}\right)g_{\mathbf{K}}g_{\mathbf{K}}^*, \tag{22}$$

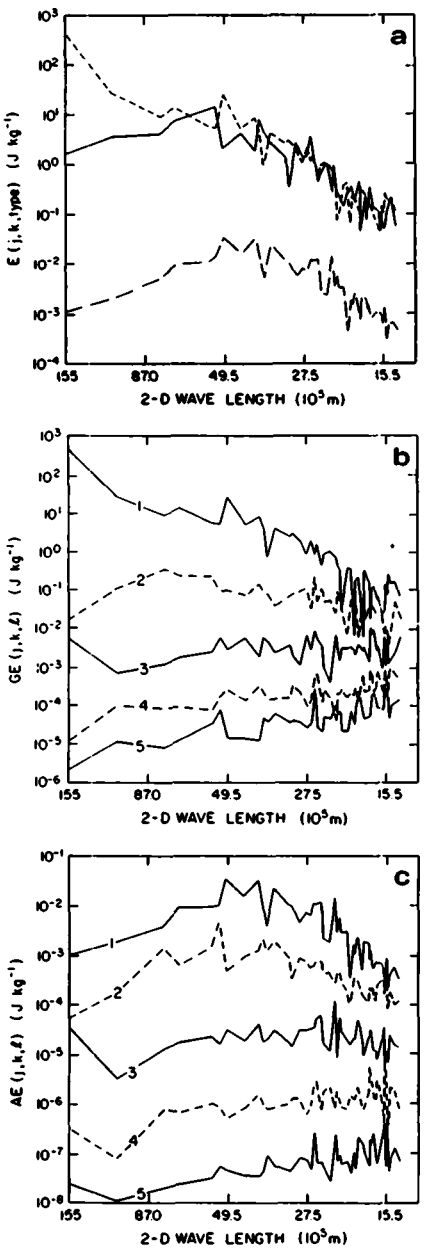

Fig. 1. (a) Initial energy spectra (units of J kg^{-1} per unit wavenumber) for the barotropic (———), baroclinic geostrophic (– – – –), and ageostrophic (— — —) modes as a function of horizontal wave length (logarithmic scale). (b) Initial energy spectra (units of J kg^{-1} per unit wavenumber) for the baroclinic geostrophic modes as a function of indicated vertical mode number and horizontal wave length. (c) Same as (b), except for ageostrophic modes.

is also conserved. This is the total QG potential enstrophy.

4. The primary experiment

The energy spectra of the barotropic, baroclinic geostrophic, and ageostrophic modes at the initial time ($t = 0$) for Exp. 1 appear in Fig. 1a as a function of horizontal wave length $2\pi D(j^2 + k^2)^{-1/2}$. These spectra are respectively similar to those of the kinetic energy of the barotropic wind (identical in this case), the available potential energy, and twice the energy of the irrotational wind. Energy spectra for the baroclinic geostrophic and ageostrophic modes are further resolved into contributions by separate vertical modes l in Figs. 1b and 1c, respectively. Since the number of modes contributing to a spectrum at any one scale varies (due to the discrete nature of the scales), the values appearing in Figs. 1a–1c are normalized by $2\pi(j^2 + k^2)^{1/2}/M_{jk}$, where M is the number of independent pairs (j,k) which yield a particular value of $j^2 + k^2$ (cf. Lin, 1982).

This initial condition was obtained from a solution to a high-resolution diabatic version of the model. That model was designed to simulate atmospheric dynamics. Thus, the spectra appearing in Figs. 1a–1c should be qualitatively similar to those of the atmosphere (assuming the latter could be defined in some similar manner; cf. Kasahara and Puri, 1981). In particular, the most energetic mode is a very large scale baroclinic geostrophic one, the barotropic spectrum peaks near the

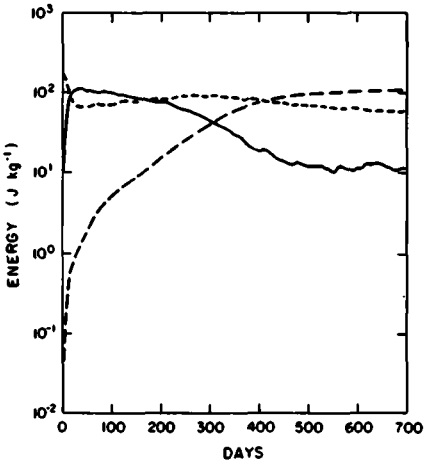

Fig. 2. The three types of energy, BE (———), GE (– – – –), and AE (— — —), as functions of time.

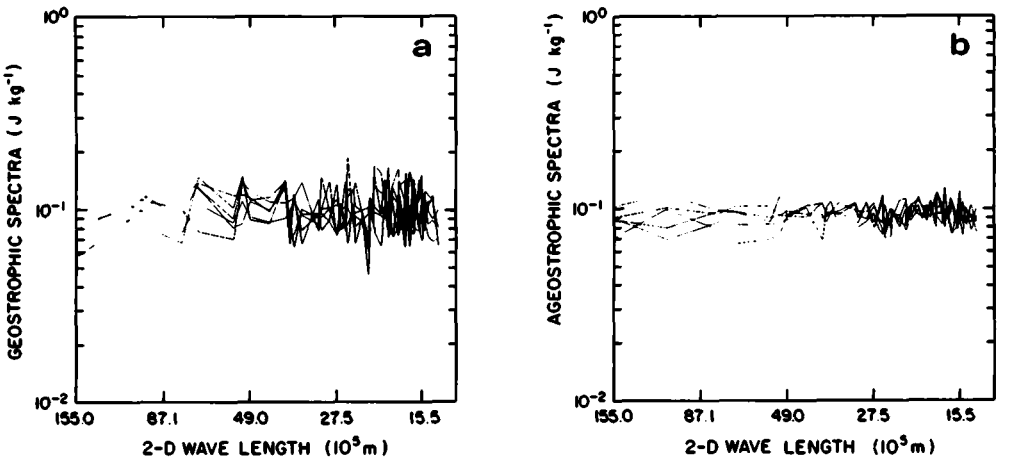

Fig. 3. Energy spectra (units of J kg per unit wavenumber) averaged over the last 40 days for (a) the geostrophic modes (b) the ageostrophic modes as a function of vertical mode l (not shown) and horizontal wave length (logarithmic scale). The spectrum of the barotropic mode is also presented in (a). Spectral values have been normalized so that exact equipartitioning would appear as a single horizontal line.

Rossby radius, and the ageostrophic modes are relatively weak.

For this initial condition, both a_K and d_K have been determined from b_K and g_K using the initialization scheme proposed by Machenhauer (1977). Specifically, a linear initialization followed by four iterations of his nonlinear scheme were used to determine all a_K and d_K. His procedure yields fields for which $da_K/dt \approx 0$ for each K (and similarly for d_K). This condition biases the solution to one that is gravity-wave free for some initial span of time.

Time series for BE, GE, and AE appear for comparison in Fig. 2. Note that after 700 days, $AE \approx 2GE \approx 10BE$. This is the relationship satisfied by an equipartitioning of energy among all the independent modes of the system (10:5:1 are the proportions of the three types of modes in this model).

Spectra for the geostrophic modes as functions of horizontal wavelength and l are presented in Fig. 3a. Spectra for ageostrophic modes are presented similarly in Fig. 3b. For this presentation, the spectral values have been divided by $M_{j,k}$ and $2M_{j,k}$ in each respective figure. Thus, exact equipartitioning would appear as a single horizontal line in these figures. (The additional factor of two in the normalization for Fig. 3b accounts for the independence of the a_K and d_K modes.) These figures confirm that this model tends to equipartition the energy, although for this specific case the process takes more than 600 days.

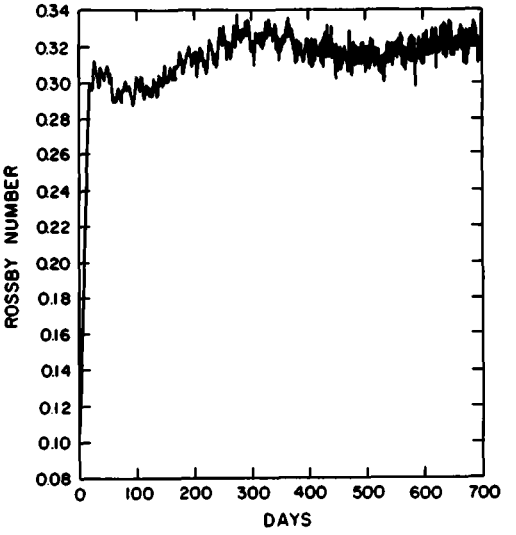

Fig. 4. The Rossby number ε as a function of time.

The time series of the Rossby number ε appears in Fig. 4. As in Errico (1982a), it is defined here as

$$\varepsilon = f^{-1}\left(\tfrac{1}{2}\sum_K \zeta_K \zeta_K^*\right)^{1/2}. \tag{23}$$

The additional factor of $\frac{1}{2}$ appears here because

$$\tfrac{1}{2} = \frac{1}{\pi H}\int_0^{\pi H} \cos^2(lz/H)\mathrm{d}z. \qquad (24)$$

The initial value of ε is 0.085. By day 15, $\varepsilon > 0.30$. Towards the end of the integration, $\varepsilon \approx 0.32$ with fluctuations of approximately 4%. This dramatic change of ε from its initially small value is consistent with the change in energy spectra during this time.

5. The initial approach toward equilibrium

From examination of only *GE* and *BE* for the first 40 days in Fig. 2, one may conclude that the solution approaches a statistical-equilibrium state not characterized by energy equipartitioning. During this period, the baroclinic geostrophic modes yield more than half their energy to the barotropic geostrophic modes. In other words, at the end of this period, most energy is in the form of kinetic energy, and the velocity field is approximately barotropic. However, examination of *AE* during this initial stage suggests that no equilibrium state has been attained in fact. In particular, at day 40, *AE* appears to be increasing with an approximate doubling time of 20 days.

This initial behaviour of Exp. 1 can be explained by comparing its solution with one obtained from a quasi-geostrophic form of the model. The *QG* model in this case is obtained by transforming from V and ϕ to normal-mode coefficients, replacing the values of a_K and d_K by zero, transforming back to the original variables, and then calculating the time tendencies. This procedure is executed at each time step of the numerical integration.

The *QG* model is run for 120 simulated days in Exp. 2. The initial condition for this experiment is obtained from that of Exp. 1 by appropriately replacing values of a_K and d_K by zero. Thus, coefficients of the geostrophic modes for both experiments are initially identical. Time series of *BE* (solid line) and *GE* (dashed line) for Exp. 2 appear in Fig. 5. They are denoted by a label 2, and are to be compared with those of Exp. 1 (labeled 1). In Exp. 2, *BE* and *GE* do not change significantly after 60 days, unlike in Exp. 1.

The solution of the *QG* model does not tend to an energy equipartioning because there are two quadratic constraints on the solution. Unlike the *PE* model, the *QG* model conserves Q as well as E

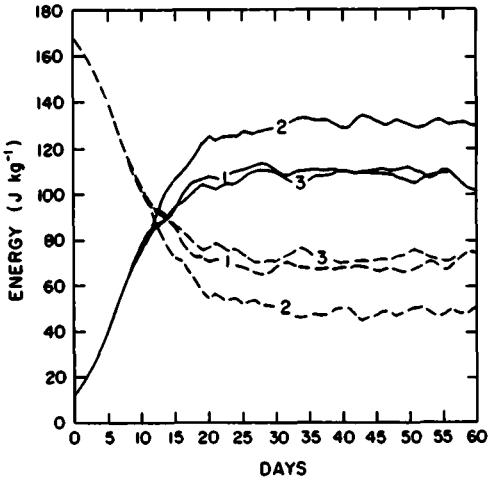

Fig. 5. Comparison of the time series of *BE* (———) and *GE* (– – – –) for the first 60 days of Exps. 1–3 (the *PE*, *QG*, and *BA* models, respectively).

(actually $E' = BE + GE$). The effects of such a pair of constraints have been described by Kraichnan (1967), Fox and Orszag (1973), Salmon et al. (1976), and Frederiksen and Sawford (1980). The present *QG* model results agree quantitatively with those of Salmon et al. (1976).

During the first 10 days, respective values of both *BE* and *GE* are similar in Exps. 1 and 2. During this time, the agestrophic modes in Exp. 1 are very weak. The solution then is approximately quasi-geostrophic. Also, the ageostrophic modes during this time are relatively slow (compared with their resonant frequencies). These results imply that the ageostrophic modes have remained approximately balanced. This conclusion is confirmed by direct calculation of both the root mean power-weighted squared frequency of the modes and the energy of the unbalanced portion of the ageostrophic field (both measures as described in Errico, 1982a). A time series of the former quantity appears in Fig. 6 for barotropic, baroclinic geostrophic, and ageostrophic modes.

Although the ageostrophic modes are weak throughout the first 40 days, their effect on some geostrophic modes may be large for reasons suggested in Errico (1982b). This effect could explain the differences between Exps. 1 and 2 at day 20. To test this hypothesis, a balanced (*BA*) model of the type described in Errico (1982b) was

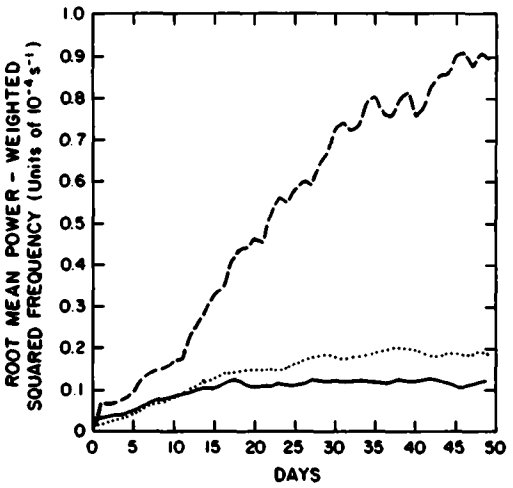

Fig. 6. The root mean power-weighted squared frequencies of the barotropic (———), baroclinic geostrophic (·····), and ageostrophic (— — —) modes as a function of time for the first 50 days of Exp. 1.

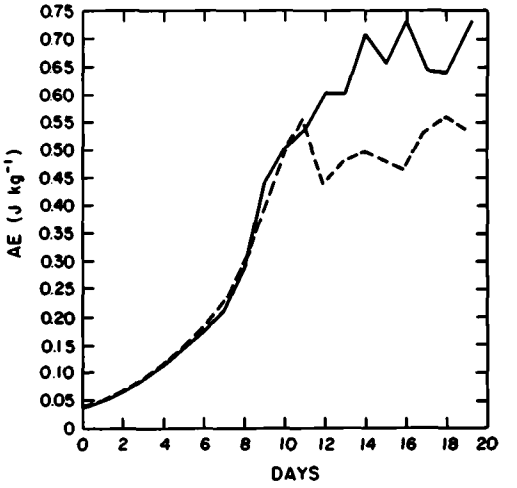

Fig. 7. Comparison of the time series of *AE* for the first 20 days of the *PE* model Exp. 1 (———) and the *BA* model (– – – –) Exp. 3.

developed. It is described in the appendix for the present model configuration. It conserves the same energy as the *QG* model (i.e., $E' = BE + GE$), but includes some effects of a balanced ageostrophic field (see the appendix).

The *BA* model was integrated for 60 days in Exp. 3. Time series of *BE* and *GE* appear in Fig. 5. They are labeled by the number 3. These series resemble those of the solution to the *PE* model more closely than those of the solution to the *QG* model. The time series of *AE* for exps. 1 and 3 appear for comparison in Fig. 7. They are very similar out to 10 days; by day 20 the former is larger by 30%. These results, along with the formerly described analyses of the ageostrophic modes in Exp. 1, confirm that the differences between the *QG* and *PE* model solutions during the first 40 days are primarily the effects of a balanced portion of the ageostrophic fields.

6. The rate of approach to equilibrium

In general, the length of time before statistical equilibrium is attained depends on details of the initial spectra. For given relative amplitudes of all the modes (i.e., shape of the spectra), the initial condition can be specified by a single number. Here, that number is chosen as ε. In the present section, the rate of approach to equilibrium is discussed as a function of ε, with the spectral shape fixed. The rate of approach is defined here as

$$\gamma(t_1,t_2) = \ln[AE(t_2)/AE(t_1)]/(t_2 - t_1). \tag{25}$$

As described in the last section, there are two primary stages of the approach to equilibrium. The first stage is dominated by quasi-geostrophic dynamics. During this stage, the growth of *AE* is relatively rapid. The second stage is one of slow growth of gravity waves (i.e., resonant-frequency ageostrophic modes). This latter stage is described below. Each stage is characterized by its own ε dependence of γ. In Exp. 1, the first 40 days may be considered as stage one, and the remaining 660 days as stage two.

6.1. *Stage one*

In the *QG* f-plane model, the time scale is determined by the quadratic advective terms. If the coefficients of all modes are scaled by the initial value of ε (denoted ε_I), and if time is scaled by ε_I^{-1}, then ε_I can be explicitly removed as a parameter in the equations. This implies that if a solution is known for a single value of ε_I, it can be determined for any value of ε_I by appropriately scaling the known solution. Thus, in the *QG* model, the rate of approach to statistical equilibrium is proportional

to ε_I if the initial relative amplitudes of the modes are fixed.

For stage one, similar scaling arguments can be applied to the *PE* model to the degree that it behaves like the *QG* model. The rate of change of the geostrophic modes is approximately proportional to ε_I. The same is true of γ.

Since the balanced a_K and d_K are quadratic functions of b_K and g_K, AE scales like ε_I^4. Thus, the change in AE during this initial stage scales like ε_I^4. However, if and when equipartioning is obtained, $AE \propto \varepsilon_I^2$. Thus, the smaller ε_I, then the greater is that change in AE which must occur during the second stage. These arguments apply only for $\varepsilon_I \ll 1$ which is a necessary condition for the *PE* and *QG* solutions to be similar initially. This scaling is more accurate for smaller ε_I.

6.2. *Stage two*

The rate of approach to statistical equilibrium during stage two is examined here in terms of the instability of the *QG* equilibrium solution to ageostrophic disturbance. In this way, it is unnecessary to repeat the integrations of stage one. The solution during that stage may be obtained approximately by rescaling the *QG* solution as described above.

Day 70 of the solution in Exp. 2 has been chosen to determine the initial conditions for Exps. 4–10. Any other day after 20 presumably would be appropriate. In each experiment, those geostrophic coefficients are multiplied by a single rescaling coefficient ε_R. They are then used as the initial geostrophic coefficients. Coefficients of the ageostrophic modes are obtained by some number of iterations N of Machenhauer's scheme (beginning from a linear initialization, denoted by $N = 0$). Values of $\varepsilon_I = 0.086\ \varepsilon_R$ and N for Exps. 3–10 appear in Table 1 (0.086 is ε_I of Exps. 1–3).

Time series of AE for Exps. 4–10 appear for comparison in Fig. 8. It is difficult to quantify the results of these experiments by looking at any single time period. γ may vary greatly with time (e.g. in Exp. 4) or with initial condition (compare Exps. 8–9 for the first 70 days). In each experiment, ε typically varies by 10% during the period of integration. Thus, interpretation of a time-mean γ as a function of a fixed ε_I is questionable.

However, several qualitative results may be obtained from Fig. 8. Smaller values of ε_I tend to be associated with smaller values of γ. This applies to the time behaviors of Exps. 4–6 also (ε decreases during the first two-thirds of the integrations for Exps. 4–10). For small ε_I, a nonlinearly-balanced initial condition (i.e., $N \geq 1$) tends to have a smaller γ initially than one that is linearly balanced ($N = 0$).

Table 1. *Initial conditions for Exps. 4–10*

Exp.	4	5	6	7	8	9	10
ε_I	0.096	0.086	0.086	0.077	0.070	0.070	0.065
N	12	9	6	6	0	4	0

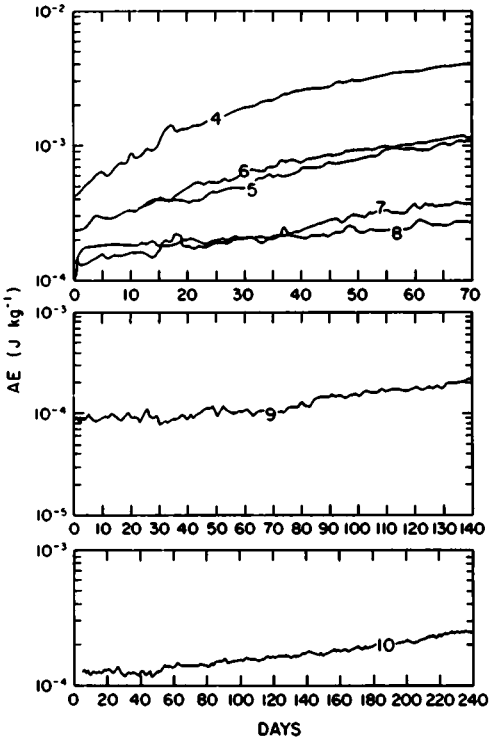

Fig. 8. Comparison of the time series of AE for Exps. 4–10.

7. Conclusions

For the primitive-equation model which has energy as its single quadratic invariant, atmospheric initial conditions yield statistical equilibrium solutions characterized by the equipartitioning of energy among all the independent linear

modes of the model. For the particular f-plane model and initial conditions used here, this equilibrium state is attained after two simulated years. The two-year transient time is characterized by at least two stages. The first stage is governed by quasi-geostrophic dynamics, during which the ageostrophic modes are relatively balanced. The second stage is characterized by the slow growth of ageostrophic motions at their resonant frequencies (i.e. of inertial gravity waves).

When started from an atmospheric initial condition, the quasi-geostrophic potential enstrophy changes very slowly in the primitive equation model. Thus, for an initial period (~40 days in the present case) the primitive equation solution resembles a quasi-geostrophic solution for which both energy and potential enstrophy are important invariants. The primary differences between the two solutions during this time are due to those ageostrophic processes which may be represented in an energy-conserving nonlinearly balanced model. During this stage, the ageostrophic energy changes greatly, but primarily due to changes in the geostrophic fields and the balanced portion of the ageostrophic fields which they determine.

The present results may be compared with some preliminary ones reported by Frederiksen (1981). He examined kinetic energy spectra obtained using a multilevel primitive-equation model on the sphere. His results suggest the relatively quick establishment of an equilibrium for rotational modes, analogous to the stage-one quasi-equilibrium described here. Thereafter, the kinetic energy spectrum tends to flatten, which suggests a tendency toward equipartitioning, also as observed here. Both of his equilibria appear to establish themselves more quickly than do the corresponding equilibria in the primary experiment here.

Small changes in the initial fields (i.e., < 20%) may greatly affect the length of time before equilibrium is attained. Two effects act in concert here. The percentage of the change in AE which occurs during the first stage as compared with that during the second stage strongly depends on the initial fields. Also, during the second stage, the instability of the geostrophic fields to ageostrophic disturbances are very sensitive to the strength of those fields. Thus, the length of time before equilibrium is attained may be quite long (many simulated years) for other atmospheric models or initial conditions. For this reason, the unstable quasi-geostrophic equilibrium attained at the end of stage one may be misinterpreted as the true equilibrium solution.

Most of the quantitative results in this paper are strongly model dependent. For models with vastly greater resolution, the proportion of energy in any mode at equilibrium will be vastly diminished. Also, the use of spherical geometry may significantly change the coefficients which describe nonlinear interactions among modes, as well as change the resonances of the types of modes (e.g., in this case rotational modes have non-zero eigenvalues). Therefore, the times for various quasi-equilibria or a final equilibrium to become established may be as greatly affected as they are by small changes in the initial conditions. However, these other models may also be expected to have equilibria solely determined by their invariants, as in the present case. With these caveats, the present results should be interpreted qualitatively, illustrating tendencies and types of equilibria.

8. Appendix

Formulation of the balanced (BA) model

A low-order version of this model is described in Errico (1982b). It can be derived formally from a *PE* model by: (1) assuming the Rossby number ε is very small ($\varepsilon \ll 1$); (2) assuming the time scale is order ε^{-1}; (3) noting that the first two conditions yield an approximate diagnostic relationship which describes ageostrophic coefficients in terms of geostrophic coefficients; and (4) retaining all terms in the prognostic equations for geostrophic coefficients through third order in ε, after substituting for ageostrophic coefficients using the relation described in step 3. Through the truncation in step 4, the relationship of step 3 becomes a pair of exact relationships. One is related to the quasi-geostrophic omega equation. The other is related to a nonlinear balance condition (e.g., to that of Haltiner, 1971). The model conserves the kinetic energy plus available potential energy of the geostrophic modes. For further details, the reader should consult Errico (1982b).

The present *BA* model has been developed from the present *PE* model by utilizing a system of transforms and filters. The procedure is as follows: (1) set $a_{\mathbf{K}} = 0$ and $d_{\mathbf{K}} = 0$ for all **K**, and then calculate $da_{\mathbf{K}}/dt$ and $dd_{\mathbf{K}}/dt$; (2) reset $a_{\mathbf{K}} =$

$-(i/\omega_K)(da_K/dt)$ and $d_K = (i/\omega_K)(dd_K/dt)$ for all K (with the filtering in step 1, this yields the desired balance condition); (3) calculate db_K/dt and dg_K/dt from the initial b_K and g_K and balanced a_K and d_K; (4) set $b_K = 0$ and $g_K = 0$ and recalculate db_K/dt and dg_K/dt; (5) finally, subtract the time tendencies calculated in step 4 from those in step 3. The last two steps remove quadratic ageostrophic-mode terms from the prognostic geostrophic-mode equations. Throughout this procedure the coefficients and their time tendencies are computed using the appropriate linear transformations of the physical fields (e.g., eqs. 9–11).

Both the *BA* and *QG* models are integrated with a time step of 1000 s.

9. Acknowledgments

The author thanks Jack Herring of NCAR and Steve Orszag of MIT for providing the initial computer code for the numerical model. The author also thanks his reviewers for their helpful comments, and Mary Niemczewski for typing the manuscript.

REFERENCES

Errico, R. M. 1982a. Normal mode initialization and the generation of gravity waves by quasi-geostrophic forcing. *J. Atmos. Sci. 39*, 573–586.

Errico, R. M. 1982b. The strong effects of non-quasi-geostrophic dynamic processes on atmospheric energy spectra. *J. Atmos. Sci. 39*, 961–986.

Fox, D. G. and Orszag, S. A. 1973. Inviscid dynamics of two-dimensional turbulence. *Phys. Fluids 16*, 169–171.

Frederiksen, J. S. 1981. Scale selection and energy spectra of disturbances in Southern Hemisphere flows. *J. Atmos. Sci. 38*, 2573–2584.

Frederiksen, J. S. and Sawford, B. L. 1980. Statistical dynamics of two-dimensional inviscid flow on a sphere. *J. Atmos. Sci. 37*, 717–732.

Haltiner, G. J. 1971. *Numerical weather prediction*. New York: John Wiley & Sons, 317 pp.

Hoskins, B. J. and Bretherton, F. P. 1972. Atmospheric frontogenesis models: mathematical formulation and solution. *J. Atmos. Sci. 29*, 11–37.

Kasahara, A. and Puri, K. 1981. Spectral representation of three-dimensional global data by expansion in normal mode functions. *Mon. Wea. Rev. 109*, 37–51.

Kraichnan, R. H. 1967. Inertial ranges in two-dimensional turbulence. *Phys. Fluids 10*, 1417–1423.

Leith, C. E. 1980. Nonlinear normal mode initialization and quasi-geostrophic theory. *J. Atmos. Sci. 37*, 958–968.

Lin, H. 1982. Weakly inhomogeneous turbulence theory with applications to geophysical flows. Ph.D. thesis, Massachusetts Institute of Technology, Cambridge, Massachusetts, 145 pp.

Lorenz, E. N. 1960. Energy and numerical weather prediction. *Tellus 12*, 364–373.

Lorenz, E. N. 1971. An N-cycle time-differencing scheme for stepwise numerical integration. *Mon. Wea. Rev. 99*, 644–649.

Machenhauer, B. 1977. On the dynamics of gravity oscillations in a shallow water model, with application to normal mode initialization. *Contrib. Atmos. Phys. 50*, 253–271.

Salmon, R., Holloway, G. and Hendershott, M. C. 1976. The equilibrium statistical mechanics of simple quasi-geostrophic models. *J. Fluid Mech. 75*, 691–703.